Journal of Power Sources 196 (2011) 10712–10716

Contents lists available at SciVerse ScienceDirect

Journal of Power Sources

journal homepage: www.elsevier.com/locate/jpowsour

Short communication

Facile synthesis and electrochemical performance of ordered $LiNi_{0.5}Mn_{1.5}O_4$ nanorods as a high power positive electrode for rechargeable Li-ion batteries

Hyun-Wook Lee [a], P. Muralidharan [a], Claudio M. Mari [b], Riccardo Ruffo [b,*], Do Kyung Kim [a,**]

[a] Department of Materials Science and Engineering, KAIST, Daejeon 305-701, Republic of Korea
[b] Dipartimento di Scienza dei Materiali, Università degli Studi di Milano-Bicocca, Milan 20125, Italy

ARTICLE INFO

Article history:
Received 27 June 2011
Received in revised form 30 August 2011
Accepted 1 September 2011
Available online 7 September 2011

Keywords:
Lithium ion battery
High voltage cathode
Lithium nickel manganese oxide
Nanorod
High rate capability

ABSTRACT

One-dimensional ordered $LiNi_{0.5}Mn_{1.5}O_4$ nanorods have been fabricated and investigated for use as a high power cathode in rechargeable Li-ion batteries. These highly crystalline nanorods, with an ordered spinel structure and diameters and lengths around 130 nm and 1.2 μm, respectively, were synthesized in two steps by using a hydrothermal reaction to produce β-MnO_2 nanorods followed by solid-state lithiation. Electrochemical analysis showed the superior performance of nanorods as a cathode in Li-ion half cells. The specific charge and discharge capacities were found to be 120 and 116 mAh g^{-1} at a 0.5 C rate, and 114 and 111 mAh g^{-1} at a 1 C rate between 3.5 and 5.0 V vs. Li^+/Li. Moreover, the nanorods exhibit high power capability, maintaining capacities of 103 and 95 mAh g^{-1} at specific currents of 732.5 and 1465 mA g^{-1} (5 and 10 C rates), respectively.

1. Introduction

In the last few years, there has been an enormous increase in the use and demand for Li rechargeable batteries with higher energy densities and power capabilities for portable electronic devices and for hybrid and all-electric vehicles. For these applications, batteries with increased energy are desired, and various alternate positive electrode materials have been widely investigated to obtain either high voltage or increased capacity [1,2]. The spinel $LiNi_{0.5}Mn_{1.5}O_4$ (LNMO) is a promising material due to its high average discharge voltage (around 4.7 V vs. Li^+/Li couple) [3–5]. In LNMO the manganese is present in its Mn(IV) valence state, and only the $Ni^{2+/4+}$ redox couple is responsible for the high voltage charge/discharge potential accompanying the insertion and extraction of Li^+ ions [6,7]. LNMO can exist in two different crystallographic structures: the cubic spinel with a $P4_332$ space group, which is called the "ordered" $LiNi_{0.5}Mn_{1.5}O_4$, and the so called "disordered" $LiNi_{0.5}Mn_{1.5}O_{4-\delta}$ with a *Fd3m* space group [8–10]. The disordered $LiNi_{0.5}Mn_{1.5}O_{4-\delta}$ has a special electrochemical behavior; the oxygen deficiency leads to the presence of manganese in the Mn(III) oxidation state, which can be oxidized to Mn(IV) at around 4 V [11], thus reducing the specific energy and inducing the distortion of the spinel structure. Moreover, in disordered LNMO impurities such as NiO and Li_xNi_yO are generally observed. On the other hand, disordered LNMO shows higher electronic conductivity than the ordered stoichiometric phase due to the presence of the $Mn^{3+/4+}$ redox couple and Ni/Mn disordering [12,13]. Therefore, the preparation of the high energy ordered LNMO structure that also has high specific power (high rate capability) is a formidable challenge in this research area.

To reach such a goal, two strategies are frequently employed: increasing the intrinsic electronic conductivity by the control of the electrode microstructure, and enhancing the Li-ion transport by reducing the bulk diffusion length in the active phase, which can be achieved by the use of nanostructured materials. Several researchers have already obtained high rate capability and cyclability through the use of nanosized materials [8,14]. In our previous work [15,16], we demonstrated that the one-dimensional (1-D) nanosized $LiMn_2O_4$ spinel phase has a superior rate capability due to a large area of contact with the electrolyte, shorter distances for Li-ion transport, and an enhancement of the electronic pathway [17]. In addition, the 1-D nanosized structure may improve the mechanical stability of the electrode compared to zero-dimensional nanosized systems (nanopowders) which tend to undergo decrepitation during electrochemical reactions [18]. Since the ordered LNMO spinel has a cubic structure, its 1-D fabrication as nanowires or nanorods appears to be a difficult task, and it has not been demonstrated until now.

In this study, we report on the preparation of ordered LNMO nanorods via a multistep synthesis: a hydrothermal reaction to

* Corresponding author. Tel.: +39 02 64485153; fax: +39 02 64485400.
** Corresponding author. Tel.: +82 42 350 4118; fax: +82 42 350 3310.
E-mail addresses: riccardo.ruffo@unimib.it (R. Ruffo), dkkim@kaist.ac.kr (D.K. Kim).

0378-7753/$ – see front matter © 2011 Elsevier B.V. All rights reserved.
doi:10.1016/j.jpowsour.2011.09.002

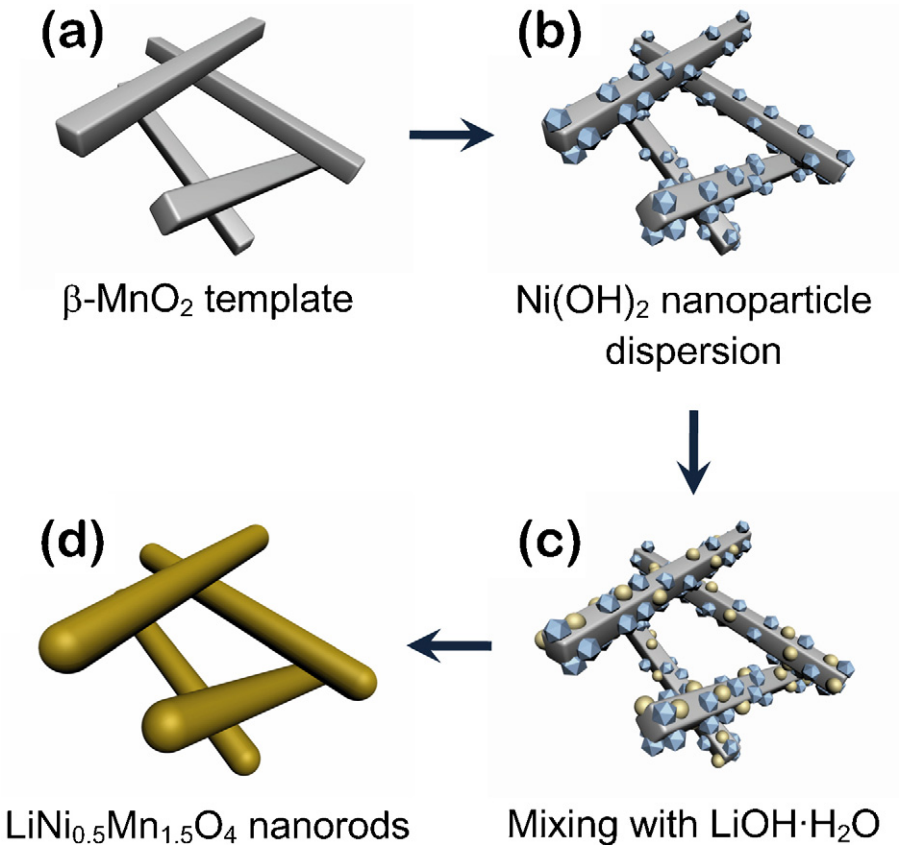

Fig. 1. Scheme of the fabrication process of ordered $LiNi_{0.5}Mn_{1.5}O_4$ nanorods: (a) β-MnO_2 nanorods obtained via hydrothermal reaction; (b) dispersion of Ni hydroxide nanoparticles on β-MnO_2 template; (c) mixing with Li hydroxide and (d) ordered $LiNi_{0.5}Mn_{1.5}O_4$ nanorods after calcination.

synthesize a beta-manganese oxide (β-MnO_2) nanorod precursor, followed by a solid-state reaction with Ni and Li precursors. The resulting LNMO structure and morphology were characterized to confirm the presence of the ordered spinel structure and the nanorod shape. The electrochemical functional characterization was carried out in half-cell vs. metallic lithium using a high voltage-stable electrolyte to evaluate the behavior of the nanorods during lithium de-intercalation and intercalation.

2. Experimental aspects

The β-MnO_2 template was prepared by hydrothermal reaction following a previously reported procedure [16]. Stoichiometric amounts of $Ni(CH_3COO)_2$ and β-MnO_2 nanorods were homogeneously dispersed in high purity ethanol and then diethylamine ($CH_2CH_2NHCH_2CH_3$) was added dropwise to increase the pH and to precipitate $Ni(OH)_2$. The dispersion was then heat treated at 120 °C to obtain a nanodispersion of $Ni(OH)_2$ on β-MnO_2 nanorods, which was subsequently mechanically mixed with $LiOH{\cdot}H_2O$ in a mortar. The final ordered LNMO nanorods were obtained by heating the mixed nanoparticle dispersion at 700 °C in an oxygen atmosphere for 8 h.

The synthesized LNMO nanorods were characterized by use of an X-ray diffractometer (XRD, Rigaku D/Max-RB (12 KW)) with Cu-Kα radiation (λ = 1.5418 Å) operating at 40 kV and 100 mA. The morphology of the nanostructure was observed by use of field emission scanning electron microscopy (FE-SEM, Hitachi S-4800) and a field-emission transmission electron microscope (FE-TEM, Tecnai G^2 F30 S-Twin). For the electrochemical investigation, 75 wt.% active material of LNMO nanorods, 17 wt.% conductive carbon black, and 8 wt.% poly(vinylidene fluoride) binder were mixed in

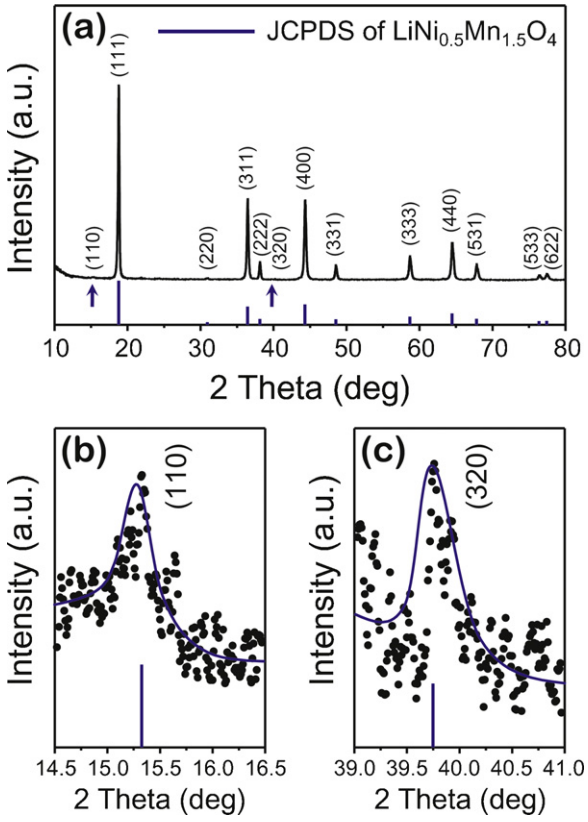

Fig. 2. XRD patterns of $LiNi_{0.5}Mn_{1.5}O_4$ nanorods: (a) comparison between powder diffraction pattern and JCPDS data No. 80-2184; (b) enlargement of (1 1 0) peak and (c) enlargement of (3 2 0) peak.

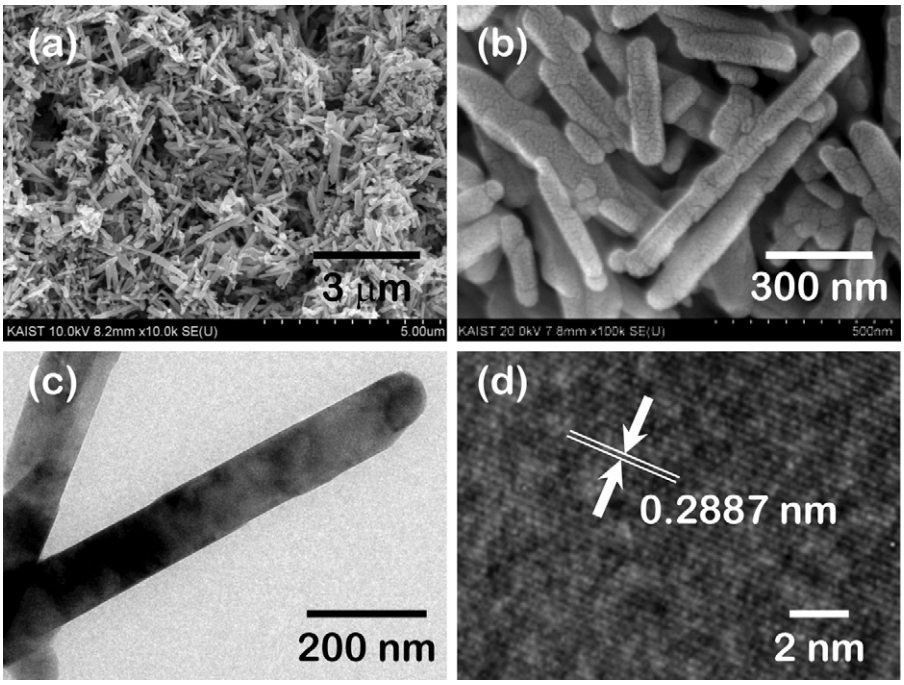

Fig. 3. Morphology of $LiNi_{0.5}Mn_{1.5}O_4$ nanorods: (a) and (b) field emission scanning electron microscopy (FE-SEM) images; (c) low magnification transmission electron microscopy (TEM) and (d) high-resolution TEM (HR-TEM) image.

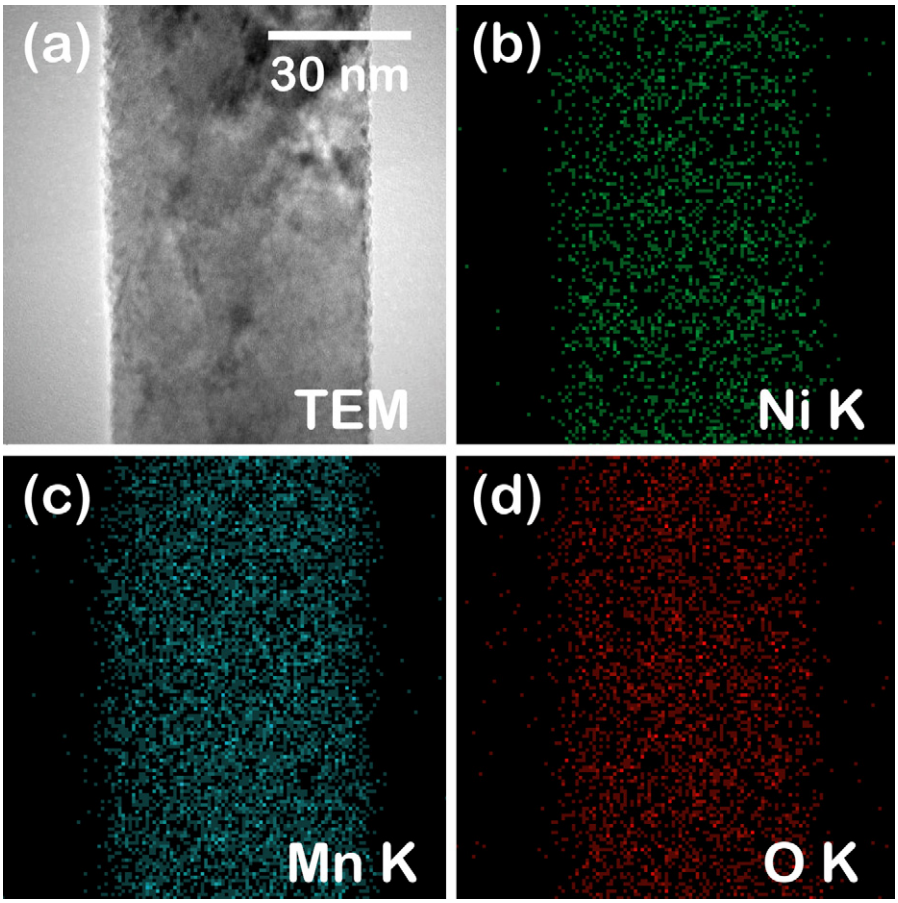

Fig. 4. TEM image and EDS mapping on a segment of a single $LiNi_{0.5}Mn_{1.5}O_4$ nanorod: (a) TEM image; (b), (c) and (d) EDS maps of Ni, Mn, and O, respectively.

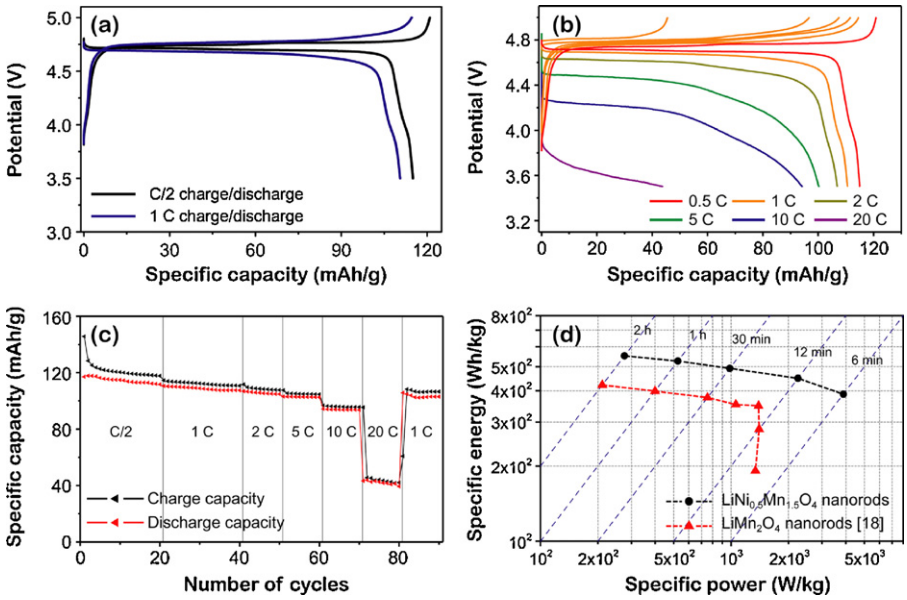

Fig. 5. Charge/discharge voltage-capacity profiles of $LiNi_{0.5}Mn_{1.5}O_4$ nanorods cycled at (a) two different C-rates (0.5, 1 C) and (b) different discharge C-rates (0.5, 1, 2, 5, 10, and 20 C); (c) specific capacity of $LiNi_{0.5}Mn_{1.5}O_4$ nanorods as a function of cycle number at different current rates and (d) Ragone plot for the synthesized $LiNi_{0.5}Mn_{1.5}O_4$ nanorods and $LiMn_2O_4$ nanorods [18].

1-methyl-2-pyrrolidone (NMP) to form a slurry, which was applied onto an etched aluminum foil current collector using a doctor-blade technique and then dried at 100 °C for 12 h. The thickness of the wet layer was 100 μm and the resulting electrode load was in the range 2.0–3.0 mg cm^{-2}. Electrochemical measurements were carried out using three-electrode type Swagelok cells assembled in a glove box filled with Ar gas ($[O_2] < 1$ ppm). Two lithium foils (Alpha Aesar) were used as both counter and reference electrodes. 1 M lithium tris(pentafluoroethyl)trifluorophosphate ($Li[(C_2F_5)_3PF_3]$) solution in 1:1 ethylene carbonate and dimethyl carbonate (EC/DMC, LF-30 Merck Selectilyte™) was employed as the electrolyte, which was supported by a glass microfiber filter separator (Whatman Inc.). Galvanostatic charge/discharge tests were performed using a BioLogic VMP3 multi-channel battery tester at room temperature.

3. Results and discussion

Fig. 1 is a schematic diagram of the synthetic procedure that was used to obtain ordered LNMO nanorods. It involved an inexpensive and scalable hydrothermal reaction (Fig. 1(a)) [16]. The nanorods are suitable powdered precursors for successive solid state reactions due to their large surface area when good dispersions with a proper reactant can be obtained. For this reason, a $Ni(OH)_2$ nanoparticle dispersion on the nanorods (Fig. 1(b)) was first prepared by precipitation of the hydroxide from an alcohol solution. The dispersion was then mixed with LiOH (Fig. 1(c)). The nanorod templates were subsequently calcined to form ordered LNMO nanorods (Fig. 1(d)). The successful synthesis of the ordered LNMO structure depends upon the dispersed state of the nickel hydroxide precipitated on β-MnO_2 nanorods.

XRD patterns of the synthesized material shown in Fig. 2(a) can be seen to match the data from the conventional spinel LNMO structure, with a $P4_332$ space group (JCPDS data No. 80-2184), and impurity peaks such as those of NiO and Li_xNi_yO are not visible. Rietveld refinement gave a lattice parameter $a = 8.167$ Å, in agreement with the value for ordered LNMO structure reported elsewhere [5]. The ordered LNMO structure has minor peaks that are usually observed at 2θ values of 15.3, 39.7, 45.7, 57.5, and 65.6°, which are defining characteristics of that structure [5]. Conversely, the disordered LNMO structure does not show such small superlattice peaks. The presence of two small peaks at 15.3 and 39.7°, corresponding to ($h\,k\,l$) Miller index (1 1 0) and (3 2 0), respectively, highlighted in Fig. 2(b) and (c), are an indication of the presence of the ordered LNMO structure. SEM images reported in Fig. 3(a) and (b) show the nanorod shape morphology of fabricated LNMO. The nanorods have an average diameter of 130 nm and a length of 1.2 μm. TEM images in Fig. 3(c) and (d) indicate that LNMO nanorods are single-crystalline. The interplanar distance determined by the HR-TEM image in Fig. 3(d) is about 0.2887 nm, which closely matches the (2 2 0) interplanar distance in LNMO. To further confirm the nanorod homogeneity, the LNMO phase was characterized by energy dispersive spectroscopy (EDS) mapping. The results, reported in Fig. 4 include a TEM image, Ni K map, Mn K map, and O K map performed on a segment of a single particle. They demonstrate that all elements are homogeneously distributed inside the bulk of the nanorod. All the structural and morphological characterizations are consistent in demonstrating that the synthesis process is able to form the ordered LNMO phase from β-MnO_2 while maintaining the nanorod morphology and size.

The battery performance of LNMO nanorod-based electrodes was measured by using 1 M $Li[(C_2F_5)_3PF_3]$ solution in 1:1 EC/DMC. The electrolyte solution of $LiPF_6$ in 1:1 EC/DMC decomposes to LiF and PF_5 under high voltage conditions, and these react with protic substances to form HF [19]; under those conditions LNMO undergoes dissolution of Mn and Ni [20–22]. For these reasons, we used the $Li[(C_2F_5)_3PF_3]$ salt which has relatively more stable bonds between P and F species [23–25]. Fig. 5(a) presents typical charge/discharge voltage-capacity profiles at two different current values. The current densities used were 73.25 mA g^{-1} (0.5 C rate, black color line) and 146.5 mA g^{-1} (1 C rate, blue color line), respectively, in the potential range 3.5–5.0 V. The voltage profiles clearly show a flat redox potential plateau around 4.75 V vs. Li/Li^+ due to the $Ni^{2+/4+}$ redox couple and characteristics of the ordered LNMO electrochemical behavior [5,8,15]. The charge profile of the disordered $LiNi_{0.5}Mn_{1.5}O_{4-\delta}$ structure shows two distinct potential regions around 4.70 and 4.76 V [5,15], which is another proof that the fabricated LNMO nanorods have the ordered spinel structure.

The specific discharge capacities were found to be about 120 and 111 mAh g^{-1} at 0.5 C and 1 C rate, respectively, showing a Coulomb efficiency around 97% at 1 C (first cycle).

The specific capacities as a function of cycle number at different rates in the voltage range of 3.5–5.0 V are reported in Fig. 5(b) and (c). The material exhibits very high rate capability, as indicated by the discharge capacity remaining almost stable up to 1465 mA g^{-1} (10 C rate). In fact, LNMO nanorods can deliver more than 100 mAh g^{-1} at a current of 732.5 mA g^{-1} (5 C), and even at 1465 mA g^{-1} (10 C), the discharge specific capacity of the nanorods was found to be about 95 mAh g^{-1}. At 2930 mA g^{-1} (20 C), it drops to 40 mAh g^{-1}. But even after this high rate measurement, the cell was able to again supply the previously delivered 146.5 mA g^{-1} (1 C) rate with capacity retention higher than 98%. This is an indication of the very good reversibility of this system. The specific energy and power of the synthesized LNMO nanorods are reported in the Ragone-type plot (Fig. 5(d)), where they are compared to spinel $LiMn_2O_4$ nanorods previously prepared in our group [17]. This plot shows that the LNMO nanorods retain their energy storage capacity to high values of power density, and that they have a higher specific energy than $LiMn_2O_4$ nanorods, as a result of the higher voltage (about 0.8 V) than that of $LiMn_2O_4$. It was mentioned earlier that 1-D morphology leads to higher particle connectivity rather than spherical nanopowders. Such interconnectivity is expected to improve the electron transport in the electrode. This merit of 1-D morphology is very important at high current rate conditions, and although the ordered materials suffer from intrinsic low electronic conductivity, LNMO nanorods retain its capacity at high current rates.

4. Conclusions

Ordered $LiNi_{0.5}Mn_{1.5}O_4$ nanorods have been fabricated by solid state reaction starting from β-MnO_2 nanorods. The key point in the preparation of the nanometric mixed oxide is the use of a suitable precursor made from the dispersion of nickel and lithium hydroxide nanoparticles onto the β-MnO_2 nanorods. The complete structural transformation to the LNMO ordered phase and the maintenance of nanorod morphology have been proved by XRD, FE-SEM, EDS mapping, and galvanostatic charge/discharge curves. Electrochemical experiments using the nanorods have demonstrated very good performance, with a stable discharge specific capacity of 95 mAh g^{-1} at 1465 mA g^{-1} (10 C). This result is a consequence of the nanometric particle size, which enhances transport properties in the bulk material, and of the large surface area of the electrode, which increases the contact with the electrolyte. As a result, the synthesized LNMO nanorods can be cycled at very high current rates in high power applications. This appears to be a promising approach to improve the rate capability in whole cells.

Acknowledgements

The work was supported by the Green Science Project of the Research Institute of Industrial Science & Technology, the Center for Inorganic Photovoltaic Materials (No. 2011-0001001), and the National Research Foundation of Korea (NRF) funded by the Ministry of Education, Science and Technology (MEST) (NRF-2010-C1AAA001-2010-0029031). Mr. Lee was financially supported by the Priority Research Centers Program through the NRF funded by MEST (2009-0094041).

References

[1] T. Ohzuku, S. Takeda, M. Iwanaga, J. Power Sources 81–82 (1999) 90–94.
[2] P. Strobel, A. Ibarra-Palos, M. Anne, C. Poinsignon, A. Crisci, Solid State Sci. 5 (2003) 1009–1018.
[3] N. Amdouni, K. Zaghib, F. Gendron, A. Mauger, C.M. Julien, Ionics 12 (2006) 117–126.
[4] Q. Zhong, A. Bonakdarpour, M. Zhang, Y. Gao, J.R. Dahn, J. Electrochem. Soc. 144 (1997) 205–213.
[5] J.-H. Kim, S.-T. Myung, C.S. Yoon, S.G. Kang, Y.-K. Sun, Chem. Mater. 16 (2004) 906–914.
[6] Y. Terada, K. Yasaka, F. Nishikawa, T. Konishi, M. Yoshio, I. Nakai, J. Solid-State Chem. 156 (2001) 286–291.
[7] S. Patoux, L. Sannier, H. Lignier, Y. Reynier, C. Bourbon, S. Jouanneau, F.L. Cras, S. Martinet, Electrochim. Acta 53 (2008) 4137–4145.
[8] K.M. Shaju, P.G. Bruce, Dalton Trans. 40 (2008) 5471–5475.
[9] M. Kunduraci, J.F. Al-Sharab, G.G. Amatucci, Chem. Mater. 18 (2006) 3585–3592.
[10] A. Bhaskar, N.N. Bramnik, A. Senyshyn, H. Fuess, H. Ehrenberg, J. Electrochem. Soc. 157 (2010) A689–A695.
[11] D. Gryffroy, R.E. Vandenberghe, J. Phys. Chem. Solids 53 (1992) 777–784.
[12] M. Kunduraci, G.G. Amatucci, J. Electrochem. Soc. 153 (2006) A1345–A1352.
[13] X. Ma, B. Kang, G. Ceder, J. Electrochem. Soc. 157 (2010) A925–A931.
[14] S.-T. Myung, S. Komaba, N. Kumagai, H. Yashiro, H.-T. Chung, T.-H. Cho, Electrochim. Acta 47 (2002) 2543–2549.
[15] H.-W. Lee, P. Muralidharan, R. Ruffo, C.M. Mari, Y. Cui, D.K. Kim, Nano Lett. 10 (2010) 3852–3856.
[16] D.K. Kim, P. Muralidharan, H.-W. Lee, R. Ruffo, Y. Yang, C.K. Chan, H. Peng, R.A. Huggins, Y. Cui, Nano Lett. 8 (2008) 3948–3952.
[17] Y. Yang, C. Xie, R. Ruffo, H. Peng, D.K. Kim, Y. Cui, Nano Lett. 9 (2009) 4109–4114.
[18] C.K. Chan, H. Peng, G. Liu, K. Mcilwrath, X.F. Zhang, R.A. Huggins, Y. Cui, Nat. Nanotechnol. 3 (2008) 31–35.
[19] A.M. Andersson, K. Edström, J. Electrochem. Soc. 148 (2001) A1100–A1109.
[20] J.Y. Shi, C.-W. Yic, K. Kim, J. Power Sources 195 (2010) 6860–6866.
[21] Y.K. Sun, C.S. Yoon, I.H. Oh, Electrochim. Acta 48 (2003) 503–506.
[22] Y. Wei, K.-B. Kim, G. Chen, Electrochim. Acta 51 (2006) 3365–3373.
[23] J.S. Gnanaraj, M.D. Levi, Y. Gofer, D. Aurbach, M. Schmidt, J. Electrochem. Soc. 150 (2003) A445–A454.
[24] J.S. Gnanaraj, E. Zinigrad, M.D. Levi, D. Aurbach, M. Schmidt, J. Power Sources 119–121 (2003) 799–804.
[25] J.S. Gnanaraj, E. Zinigrad, L. Asraf, M. Sprecher, H.E. Gottlieb, W. Geissler, M. Schmidt, D. Aurbach, Electrochem. Commun. 5 (2003) 946–951.